frontiers | Frontiers in Marine Science

TYPE Original Research
PUBLISHED 13 November 2023
DOI 10.3389/fmars.2023.1296509

OPEN ACCESS

EDITED BY
Valerio Matozzo,
University of Padua, Italy

REVIEWED BY
Ajith Kumar T. T.,
National Bureau of Fish Genetic Resources (ICAR), India
Ardavan Farhadi,
Hainan University, China

*CORRESPONDENCE
Chun-Yan Ma
macy@ecsf.ac.cn
Zhi-Qiang Liu
18817775160@163.com

†These authors have contributed equally to this work

RECEIVED 18 September 2023
ACCEPTED 24 October 2023
PUBLISHED 13 November 2023

CITATION
Xu L-K, Ma K-Y, Zhang F-Y, Wang W, Ma L-B, Jin Z-W, Zhao M, Chen W, Fu Y, Ma C-Y and Liu Z-Q (2023) Observations on the embryonic development of the mud crab, *Scylla paramamosain*. *Front. Mar. Sci.* 10:1296509. doi: 10.3389/fmars.2023.1296509

Observations on the embryonic development of the mud crab, *Scylla paramamosain*

Li-Kun Xu[1,2†], Ke-Yi Ma[1†], Feng-Ying Zhang[1], Wei Wang[1], Ling-Bo Ma[1], Zhong-Wen Jin[3], Ming Zhao[1], Wei Chen[1], Yin Fu[1,2], Chun-Yan Ma[1*] and Zhi-Qiang Liu[1*]

[1]Key Laboratory of East China Sea Fishery Resources Exploitation, Ministry of Agriculture and Rural Affairs, East China Sea Fisheries Research Institute, Chinese Academy of Fishery Sciences, Shanghai, China, [2]College of Fisheries and Life Science, Shanghai Ocean University, Shanghai, China, [3]Ningbo Yifeng Aquaculture Co. LTD, Ningbo, China

To investigate the embryonic development of the mud crab *Scylla paramamosain*, we analyzed three critical parameters: egg color of, embryo morphology (through conventional and laser scanning confocal microscopy), and the distribution of cell divisions. During embryonic development, the egg color exhibited a progressive transition, shifting from orange to reddish-orange, then to brown, before ultimately darkening to black. Each embryo displayed a spherical shape, measuring approximately 280 μm in diameter, characterized by a smooth surface devoid of any depressions. The embryonic cell division was in the form of mixed oogenesis, comprised of complete division in the early stage, spiral oogenesis in the middle stage and surface division in the late stage. It is noteworthy that the blastopore appeared at the position where the transparent area and cell aggregation just appeared under the microscope, and the blastomere was a characteristic of the embryo entering the gastrulation stage. After entering the gastrulation stage, the cells aggregated towards the blastopore and formed two symmetrical cell clusters, which formed a V-shape with the void of the classic blastopore. When the transparent region occupied approximately 1/5 of the embryo's volume, the embryo entered the nauplius stage, and the thoracic and abdominal armor, as well as the optic lobe and abdominal limb primordia, could be clearly distinguished. The appearance of the compound eye pigment band indicated the stage of compound eye pigment formation. At this time, the transparent area accounted for 1/4 of the embryo and a large number of ganglia appeared. The change of the compound eye pigment band from red to black was also one of the reasons for the blackening of the egg color of the crabs. The data obtained through this study have potential applications in the determination of embryonic development status and obtaining of high-quality seeds for *S. paramamosain* culture.

KEYWORDS

crustacean, *Scylla paramamosain*, cleavage, blastopore, embryonic development

1 Introduction

The mud crab *Scylla paramamosain* (Crustacea, Decapoda, Portunidae, *Scylla*) is one of the most important marine crab species widely cultured along the coasts of southern China, and is also an important inshore fishery resource for many countries in the Indian and Pacific Oceans (Takano et al., 2005; Ma et al., 2011). In China, the aquaculture and fishing yield of *S. paramamosain* exceeded 220 thousand tons in 2022 (Bureau of Fisheries and Fishery Management, 2023). However, despite its high economic value, the production of *S. paramamosain* has not yet been able to meet the growing demand of the consumer market. Therefore, there is an urgent need to further increase the production. Until now, there are still many scientific and technological problems that have not yet been effectively solved in *S. paramamosain* culture. In particular, the development of *S. paramamosain* culture requires a large amount of crablets. However, these seeds for *S. paramamosain* artificial farming mainly come from wild source supplements (Azra et al., 2015). The inconsistent supply and unreliable quantity of the natural seedings hinders the sustainable development of *S. paramamosain* culture.

Embryonic development is a key step in the crab breeding process and has significant effect on the growth and development of the crab individual. In the context of the urgent need for upgrading and expansion of the *S. paramamosain* culture industry, as well as the urgent need to break through the problems of low survival rate and unstable yield in nurseries, it is necessary to systematically study the embryonic development of *S. paramamosain*. Currently, studies on this crab species have focused on the genetic structure of geographic populations, comparison of differences among geographic populations, molecular markers (Lu et al., 2009; Ma et al., 2011; Ma et al., 2012; Liu et al., 2018), the effects of nutrient regulation on growth and development (Xu et al., 2020; Farhadi et al., 2022; Luo et al., 2023), as well as cloning and validation of functional genes, e.g. genes related to sex determination regulation, genes for various enzymes, and immune-related genes (Wan et al., 2021; Wang et al., 2021; Zhang et al., 2021; Ma and Zhu, 2021). In addition, the range of adaptiveness to environmental factors, such as temperature, salinity, light and dissolved oxygen content, the effects of changes in environmental factors on growth and development (Chen et al., 2021; Yao et al., 2021; Ji et al., 2022), as well as histology level (Wang et al., 2022), have been mostly studied. In contrast, studies on systematic morphological observation of the whole embryonic development period of *S. paramamosain* have seldom been reported.

There is a long history of research on the morphology of crustacean embryos and researchers have accumulated a large amount of valuable information to describe the embryo morphology. The study of crustacean embryology began in 1888 with morphological observations and descriptions of the internal structure of embryos in species with large fertilized eggs, such as trachypods and decapods, using freehand sectioning (Anderson, 2013). Tissue sectioning techniques became widely used in the study of decapod crustaceans in the 20th century. In particular, the paraffin sectioning technique is still used today by some crustacean developmentalists to characterize the histological changes in the embryo (Mann and Hyne, 2008), the neural organs (Chansela et al., 2012), the yolk sac, and many other aspects of organogenesis (Wu et al., 2009). As technology advanced further, transmission electron microscopy (TEM) began to be employed for observing the internal ultrastructure of objects of study. For instance, TEM has been used to study the ultrastructure of fertilized eggs and early crustacean embryos (Hubble and Kirby, 2007). In addition, confocal laser scanning microscopy (CLSM) has become one of the popular instruments to build up 3D images for cell analysis. For example, CLSM has been used to successfully analyze the morphological characteristics of cell migration in *Bythotrephes longimanus* from the beginning of oocyte cleavage to the 16-cell stage (Alwes and Scholtz, 2014).

For *S. paramamosain*, the mode of cell division and the process of cell migration and differentiation during embryonic development have yet to be adequately explored owing to difficulty in taking photos in the early stage. The embryo is the starting point of individual development, and in-depth study of the embryo's development can help in understanding the biology of individual development and obtaining sufficient and high-quality *S. paramamosain* seedings. Therefore, in this study we describe the observations on the important events in the development of the *S. paramamosain* embryo from fertilized egg to the hatching preparation stage, focusing on observations regarding egg color change, morphology of the embryonic development under microscope, and distribution of cell division using CLSM.

2 Materials and methods

2.1 Experiment animals

In our study, ten pairs of healthy and high-quality male (weight 415 ± 30g, carapace length 80.70 ± 6.10mm, carapace width 117.40 ± 8.21mm) and female (weight 375 ± 20g, carapace length 85.73 ± 5.03mm, carapace width 124.01 ± 7.22mm) *S. paramamosain* parents were obtained fromthe *S. paramamosain* genetic breeding innovation team of the East China Sea Fisheries Research Institute of the Chinese Academy of Fishery Sciences, Ninghai Experimental Center, Zhejiang Province. All the crabs were temporarily kept in a 4×8 m cement pond with a water depth of 50 cm, and with a shade net covering over the pool. An inflatable pump continuously aerated the water body. The water temperature was 26-28°C, and the salinity was 24-28‰. All the crabs were fed with fresh clams daily, and the water was exchanged by 1/3 once a day to maintain the freshness of the water in the pond. Before mating, the male would hold the female that was about to undergo a reproductive molt. Once the reproductive molt occurred, the male would immediately mate with her and transfer the sperm from his body to the spermathecae of the female, and then the mating was completed. The abdominal region of the female crab changed significantly after mating (Supplementary Figure 1). The umbilicus of an unmated female was relatively narrow, while that of a mated female was bluntly rounded with bristles appearing on the edge of the umbilicus. After mating, the males were removed from the pond. After spawning, six ovigerous crabs were

immediately transferred to a black incubation vat with the same temperature and salinity seawater as described above. The seawater in the vat was replaced every day to clean away the excreta and residual feeds. During this period, the overall egg color of the ovigerous crabs were photographed and recorded. Meanwhile, the embryos were checked every 30 min. The embryos at blastocyst stage, gastrulation stage, nauplius stage, compound eye pigment formation stage and the stage of preparation for hatching were collected and fixed with 4% paraformaldehyde.

2.2 Embryo sampling

Upon collection, the embryos were placed in a Petri dish containing 1× PBS solution and brought under a light microscope for observation and photographing. In the meantime, some embryo samples were fixed in 4% paraformaldehyde solution and stored at 4°C overnight.

2.3 Embryonic nucleus staining

After fixation with paraformaldehyde solution, the embryos were rinsed with 1× PBS three times and stored in pure methanol until use. The staining procedure was carried out with Sytox® Green (Molecular Probes) according to the procedure from a previous study (Ma et al., 2019). Generally, all the embryo samples were gradually rehydrated in methanol, with gradient concentrations of 90%, 80%, 70%, and then 50%, for 5 min in each concentration. Next, all the samples were rinsed thrice using PBST solution (1× PBS with Tween 20). Then, the embryos were stained in Sytox® Green with dilution of 1:20,000 for 3 h. Subsequently, the stained embryos were rinsed twice with PBST solution for 30 min and placed on a microscope slide (Sigma-Aldrich, USA). After adjusting angle of the embryos on the slide, we observed the embryos with a laser scanning confocal microscope (Olympus, Japan), and photographed them.

3 Results

The typicall developmental characteristics of the *S. paramamosain* embryo are summarized in Table 1.

3.1 Fertilized eggs and cleavage stage

The cleavage stage is the time between the fertilized egg and the blastocyst stage, when the fertilized egg develops to the blastocyst stage after eight divisions. At fertilization, the overall egg color of the crabs was clearly yellowish (Supplementary Figure 2A). The fertilized eggs, each about 280 μm in diameter, were spherical in shape, medium-yolked, smooth and without cracks. The nucleus located in the center of each embryo was encapsulated by a layer of yolk, and the dark brown spots on the surface were the cell poles (Figure 1A). The surface of the embryo was wrapped by a transparent secondary membrane, in addition to the yolk membrane that encapsulates the yolk. This secondary membrane plays both protective and adhesive roles during the egg laying process, in which the eggs would be pulled by the bristles in the umbilicus of the mother crab, before becoming attached to the setae on the mother crab's abdomen (Figure 1A). For the embryos stained with sytox, the nuclei did not have obvious fluorescence, but the cell poles on the surface did display obvious fluorescence (Figure 1B).

The first cleavage of the embryo was an inward depression of the fertilized egg, splitting the embryo into two cells, or blastomeres, of different sizes (Figure 1C), which was similar to the corresponding cell division in spot prawns (Biffis et al., 2009). In accordance with a previous study (Hertzler, 2005), we named the larger and smaller blastomeres as CD and AB, respectively (Figure 1C). During this 2-cell period, there were distinct fluorescent dots present on the embryo (Figure 1D). In addition, the first round of division of the fertilized egg did not have a significant cleavage sulcus, compared to the one that would form the 4-cell stage.

TABLE 1 Representative characteristics during embryonic development in the *S. paramamosain*.

Embryonic stage		Representative characteristic
Cleavage	1-cell	yellowish, smooth and without cracks, cell poles obvious
	2-cell	split into two cells of different sizes by the cleavage sulcus
	4-cell	cleavage sulcus obvious, cell numbers countable, with two brownish-black dots
	8-cell	cleavage sulcus obvious, cell numbers countable, a larger cell surrounded by crown cells
	16-cell	(same as above)
	32-cell	cleavage sulcus obvious, cell numbers countable
	64-cell	cleavage sulcus unclear, cell numbers countable
	128-cell	cleavage sulcus very unclear, cell numbers hard to count
Blastocyst		cleavage sulcus disappeared, uniformly distributed nuclei recessed inward along the embryo major axis
Gastrulation		blastopore and many cell clusters (VPR, OL, MN etc.) appeared
Nauplius		embryo overall size increased, semicircular ventral limb primordia appeared,
Abdominal limb formation		abdominal limb primordia differentiated into abdominal limbs
Compound eye pigmentation		heart, ventral nerve cord and two reddish-brown bands of compound eye pigment appeared
Pre-zoea (preparation for hatching)		color changed to black, embryonic develop complete, new larva fully formed

10.3389/fmars.2023.1296509

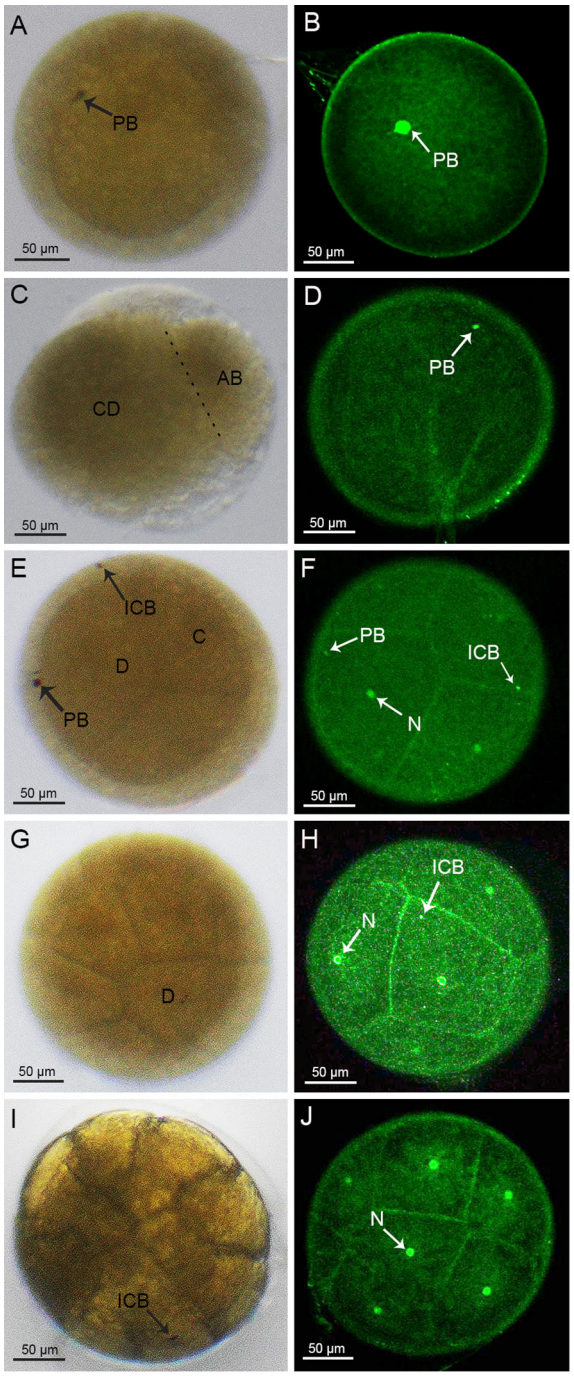

FIGURE 1
Cleavage stages of *S. paramamosain* embryos: from 1-cell to 16-cell stages. **(A, C, E, G, I)** were observed under light microscopy. **(B, D, F, H, J)** were observed under a laser scanning confocal microscope. PB, polar body; ICB, intracellular body; N, nucleus.

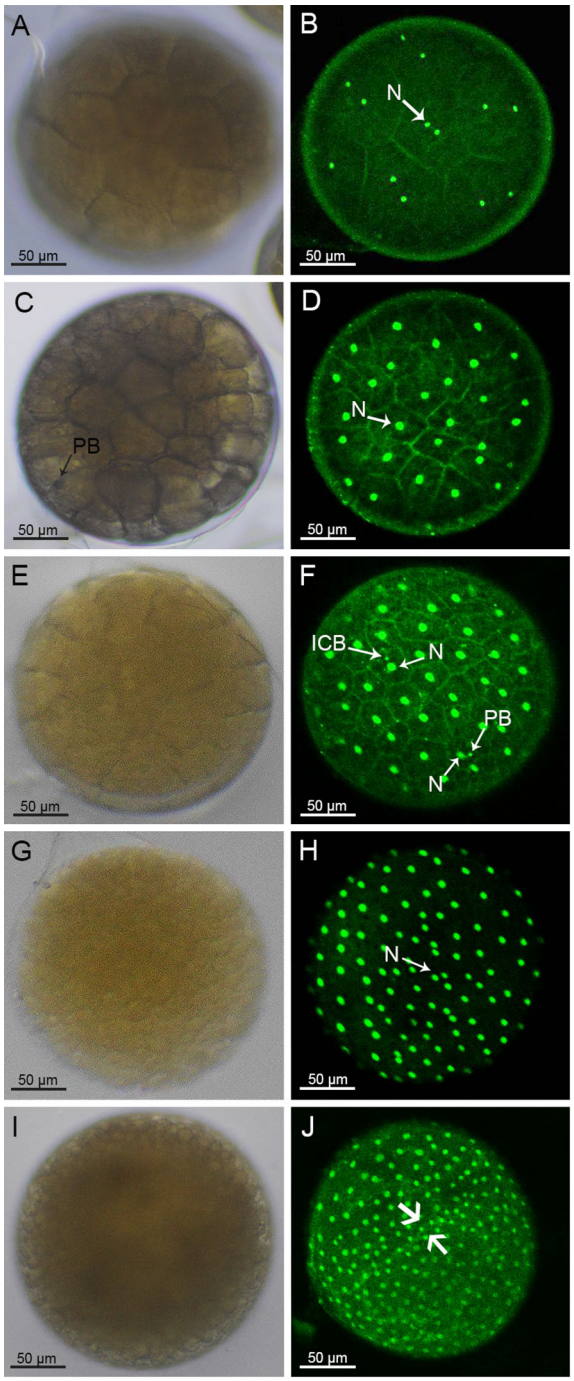

FIGURE 2
Morphology of 32-cell stage to blastocyst of *S. paramamosain* embryos under light microscopy **(A, C, E, G, I)** and a laser scanning confocal microscope **(B, D, F, H, J)**. The blastocyst stage embryo concaved in the direction of the arrow **(J)**. PB, polar body; ICB, intracellular body; N, nucleus.

The following 2nd to 6th rounds of division were in the form of spiral oogenesis, dividing the embryo sequentially into 4, 8, 16, 32 and 64 cells (Figures 1E, G, I, 2A, C). The 7th to 8th rounds of division changed from spiral oogenesis to embryonic surface oogenesis.

At the 2nd round of division, the CD blastomere divided into a C blastomere and a D blastomere while the AB blastomere divided into an A blastomere and a B blastomere (Figure 1E). At the 4-cell stage, two brownish-black dots appeared on the surface of the embryo suggesting that the larger black dot on the surface of the D blastomere was an intracellular body and the black dot on the surface of the embryo was a polar body. Moreover, two smaller fluorescent dots other than the nucleus were also observed on the

10.3389/fmars.2023.1296509

surface of the embryo (Figure 1F). At the 8-cell stage, a larger cell, surrounded by crown cells, was observed (Figure 1G). A similar pattern was observed at the subsequent 16-cell stage, where brownish-black dots appeared on the larger cells (Figure 1I). For the 4-cell to 128-cell stages (Figures 1E-J, 2A-F), the number of cells was increased, and the oval groove disappeared after the 128-cell period.

3.2 Blastoderm and gastrulation stage

After the 8th cleavage, the *S. paramamosain* embryo entered the blastocyst stage, in which many nuclei were distributed on the surface of the embryo (Figure 2H). Additionally, the cleavage furrow on the embryo surface was difficult to visualize (Figures 2G-J). At the late blastocyst stage, the uniformly distributed nuclei began to recess inward along the major axis of the embryo (Figure 2J). Unfortunately, the position of the intracellular body and the cellular polar body were not clearly observable during this period.

In the early stage of gastrulation, the blastopore was formed because of the migration of some cells into the endosomes. Due to the dense aggregation of cells, the yolk around the blastopore was rapidly consumed in comparison to the areas where the cells were more dispersed. Hence, a transparent area appeared where the blastopore was located (Figure 3A). It could be clearly observed that the blastopore had taken shape, based on the small pore formed by cell aggregation in the embryo (Figure 3B). With further development, the transparent region was enlarged and inverted triangularly concave toward the inner part of the embryo (Figure 3C). At this period, a large number of cells around the blastopore were found to be aggregated into clusters on the surface of the embryo, and the nuclei of the cells in the region were small and densely packed, whereas the cells in the region outside the blastopore were larger and more loosely arranged (Figure 3D). After the blastopore's appearance, the transparent region of the embryo was elongated toward both ends into a crescent shape, and the yolk color above the concavity of the transparent area became lighter, showing that there were cell clusters in this area (Figure 3E). The cell cluster around the blastopore (called Ventral plate rudiment, VPR) divided continuously and gradually surrounded the blastopore. In addition, another two cell clusters (called optic lobe primordia, OL) also appeared above the VPR. Usually, the VPR and OL spatially form a V-shape (Figure 3F). Next, the transparent zone of the embryo expanded to the periphery. At the same time, the color of the inner area of the transparent region was further lightened (Figure 3G). More cell clusters appeared between the OL and VPR, and these cell clusters subsequently developed into the mandible (MN) and maxilliped (MX) primordia (Figure 3H). The area of the intermediate cells, with sparser cell distribution, developed into the stomodaeum (ST) (Figure 3H). With further cell division, transparent areas were reduced in size compared to the previous stage, and the color fading was more pronounced (Figure 3I). The MN primordia, MX primordia and VPR joined together to form a single body called the thoracoabdominal fold, TF, and from the left and right sides of the TF would emerge the antennal (AL) primordia (Figure 3J).

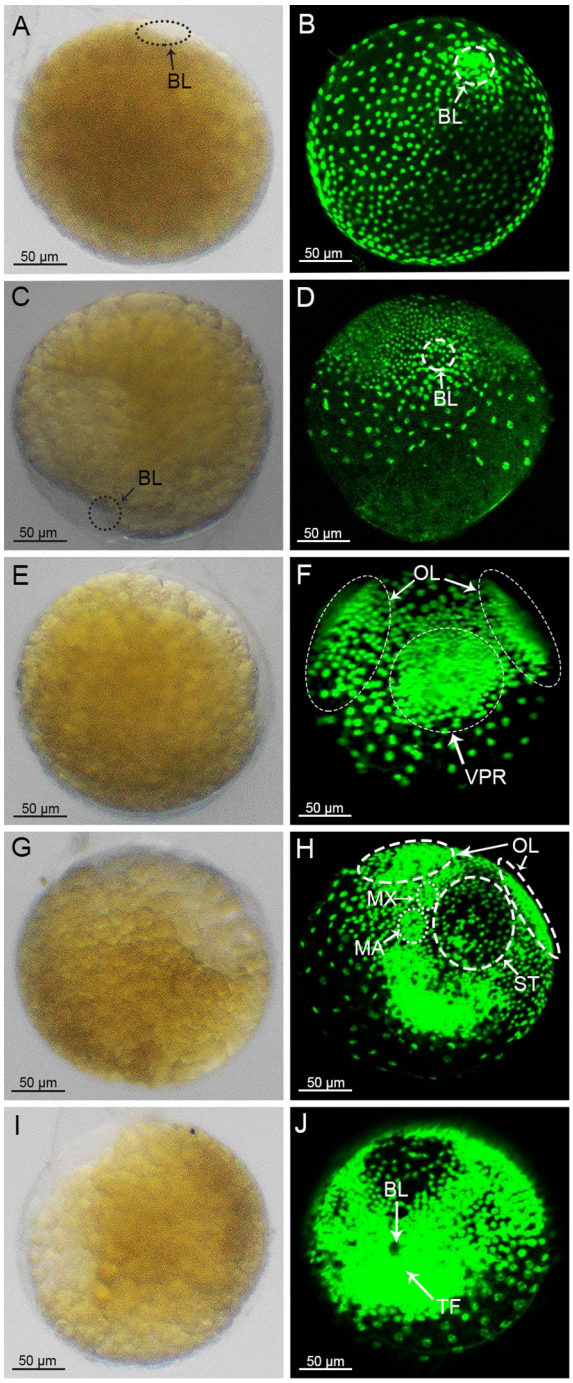

FIGURE 3
Morphology of embryos during the gastrulation stage under light microscopy **(A, C, E, G, I)** and laser scanning confocal microscope **(B, D, F, H, J)**. OL, optic lobe primordium; VPR, ventral plate rudiment; TF, thoracoabdominal fold; BL, blastopore; MN, mandibular; MX, maxilliped; ST, stomodaeum.

3.3 Nauplius stage and abdominal limb formation stage

Following the gastrulation stage, the embryonic development entered the Nauplius stage. The whole egg changed its color from orange-red to orange-yellow (Supplementary Figures 2B, C), and the overall size of the embryo increased significantly compared with the previous developmental stage. The transparent area of the embryo was crescent-shaped and accounted for about 1/5 of the egg. Part of the semicircular ventral limb primordia could be seen within the transparent area (Figure 4A). Moreover, distinct zonation occurred on the TF and evolved into distinct protostomes. From the top to bottom as shown in Figure 4B, these were the OL, MN, MX, AL, first maxilliped primordia (FMA), second maxilliped primordia (SMA), and caudal papilla (CP). Thereafter, the transparent region of the embryo occupied about 1/4 of its

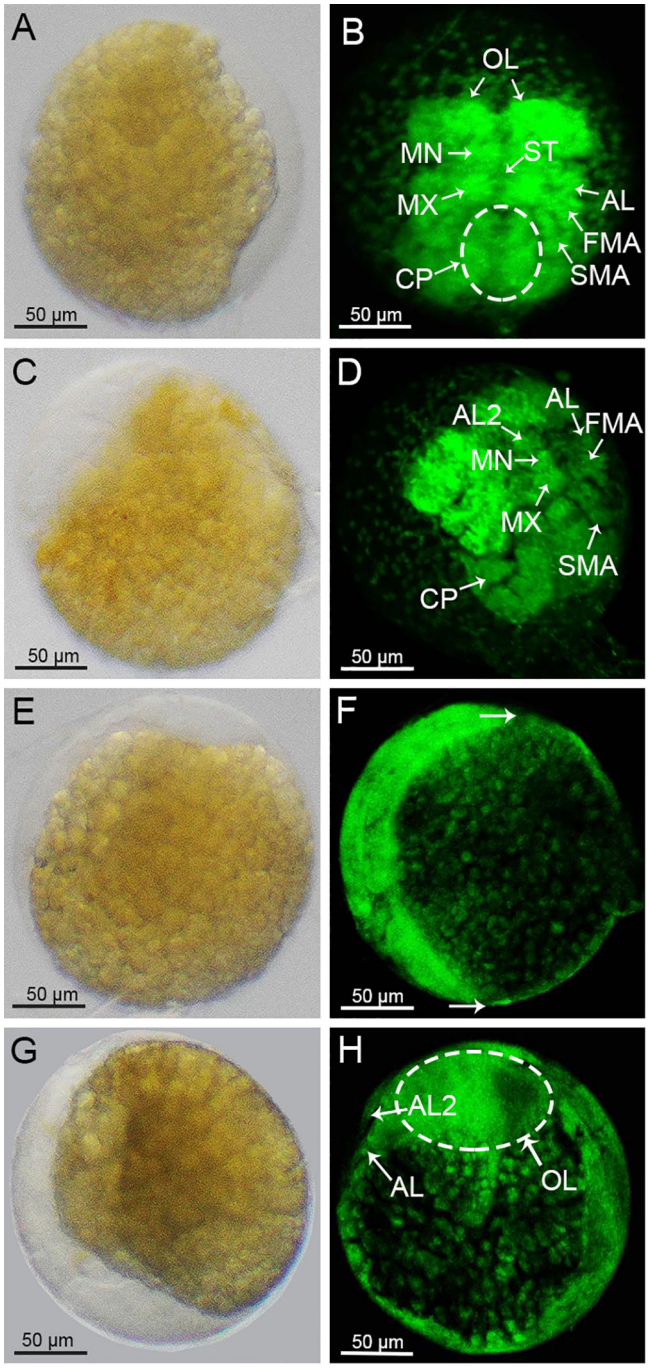

FIGURE 4
Morphological changes of the *S. paramamosain* embryos at nauplius stage. **(A, C, E, G)** were observed under a light microscopy. **(B, D, F, H)** were observed under a laser scanning confocal microscope. The hemispherical was indicated by the arrow **(C)**. OL, optic lobe primordium; MN, mandibular; MX, maxilliped; ST, stomodaeum; FMA, first maxilliped primordium; SMA, second maxilliped primordium; CP, caudal protopod; AL2, antennule tentacles.

volume, and wavy projections appeared within the transparent region (Figure 4C). The elongated ends of the FMA and SMA diverged, and the CP lengthened to evolve a ventral segmental partition, with an inwardly curved end (Figure 4D). Later, the nauplius wrapped around the yolk in an arc shape and extended to both ends (Figures 4E, F). Then the crescent-shaped transparent zone continued to expand into the inner yolk (Figure 4G). Meanwhile, the abdominal limbs gradually differentiated from the abdominal limb primordia, and the optic lobe primordia extended radially towards the two sides of the embryo (Figure 4H).

3.4 Compound eye pigment formation and preparation for hatching

With the extension of the optic lobe primordia, two reddish-brown bands of compound eye pigment radially appeared on both sides of the embryo, which was a sign that the embryo had reached the stage of compound eye pigment formation (Figure 5A). The boundaries of the thorax and the abdomen appeared to be differentiated by the position of the prothorax (Figure 5B). The pigmented bands of the compound eyes gradually thickened and deepened in color (Figure 5C). Another pair of antennule tentacles (AL2) appeared anterior to the compound eyes, and specific morphological structure appeared in the MN and MX primordia, with the FMA and SMA becoming elongated and segmented (Figure 5D). Subsequently, a large number of black ganglia appeared on the abdomen, cephalothorax, and base of the appendages of the embryo (Figure 5E). The compound eyes increased in size to about one-half the size of the embryo, and reticular zoning appeared on the surface of each compound eye. The heart appeared at the base of the compound eyes, and striated tentacles appeared at the anterior end of the compound eyes (Figure 5F). The ventral nerve cord (VNC) could be observed, wrapped around the sides of the gut and running from the protoconch to the caudal end (Figure 5G). Three pairs of appendages were clearly distributed on both sides of the abdomen, the longest of which was FMA, followed by the SMA, and the shortest being AL (Figure 5H). At this time, the overall egg color of the embryos gradually changed from brown to black (Supplementary Figures 1D-F). The yolk was rapidly consumed and contracted to form a butterfly shape (Figure 5K), which accounted for about one-half of the egg (Figure 5I). The AL curled inward and began to segment internally and externally (Figure 5J). The TF extended to differentiate the thorax and abdomen. As the abdomen emerged, the end of the abdominal segment also began to diverge (Figure 5L). After this stage, the mother crab would user her stepping feet to pluck the egg particles away from the setae to which they had been attached, freeing them into the water, where the larvae would break through their egg membranes and develop into the zoea I stage (Supplementary Figure 3).

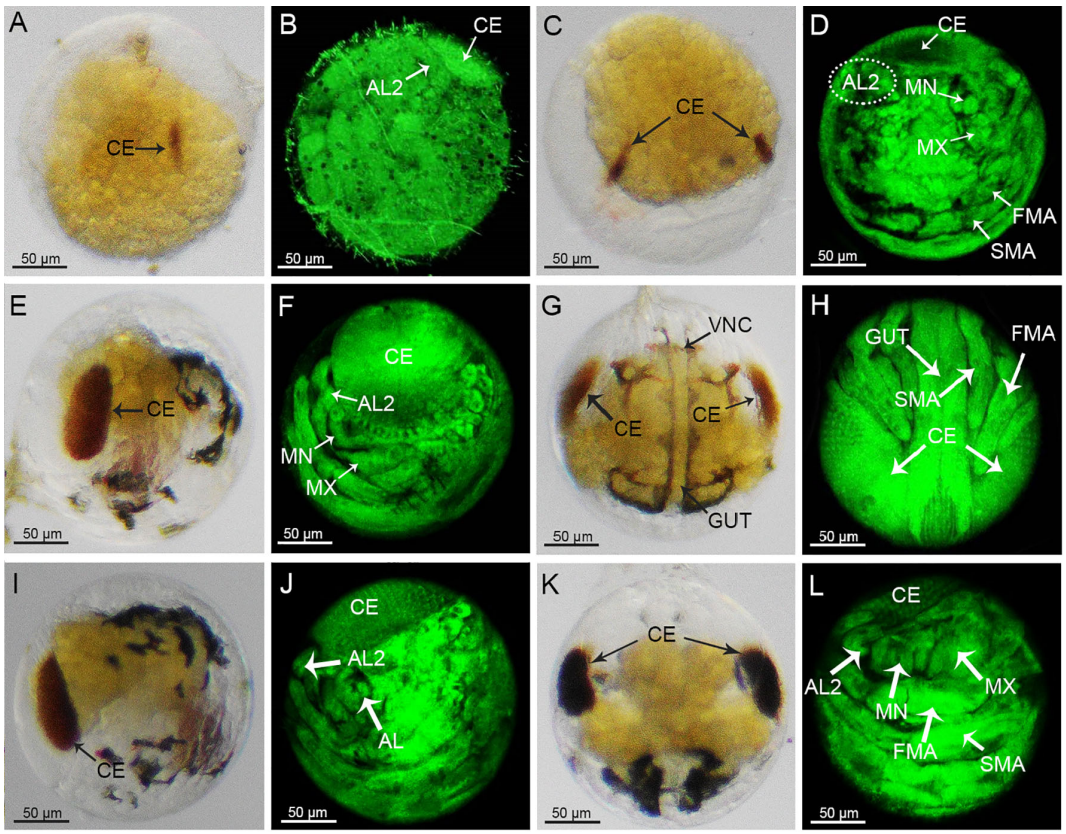

FIGURE 5
Morphological changes of embryos during the compound eye pigmentation stage to the pre-zoea I stage under light microscopy **(A, C, E, G, I, K)** and laser scanning confocal microscope **(B, D, F, H, J, L)**. AL, antennule; AL2, antennule tentacles; MN, mandibular; MX, maxilliped; FMA, first maxilliped primordium; SMA, second maxilliped; primordium; VNC, ventral nerve cord.

TABLE 2 Embryonic development in different species.

Crustaceans	Stage	Reference
Bythotrephes longimanus	Fertilized eggs, 2cell, 4cell, 8cell, 16cell	Alwes and Scholtz, 2014
Macrobrachium nipponense	Fertilized eggs, cleavage stage, blastoderm stage, gastrulation stage, nauplius stage, zoea stage	Ma et al., 2019
Penaeus monodon	Fertilized eggs, 2cell, 4cell, 8cell, 16cell, 32cell, 64cell, 122cell, gastrulation stage	Biffis et al., 2009
Litopenaeus vannamei	Fertilized eggs, 2cell, 4cell, 8cell, 16cell, 32cell, 64cell, 122cell, 244cell, Later stages of gastrulation	Hertzler, 2005
Scylla olivacea	Fertilized eggs, blastoderm stage, gastrulation stage, 3 days embryo, 4 days embryo, 5 days embryo, 6 days embryo, 7 days embryo	Azra et al., 2015
Scylla serrata	Fertilized eggs, cleavage stage, blastoderm stage, gastrulation stage, nauplius stage, 5 pairs of appendages stage, 7 pairs of appendages stage, eye-pigment formation stage, prehatching stage, hatching stage	Chen, 2007

4 Discussion

The whole process of embryonic development is basically independent of the mother and develops regularly, and the organs and systems are basically fully developed and finalized at the late stage of embryonic development. Therefore, it is necessary to carry out an in-depth and systematic study on this key link of embryonic development to clarify the internal mechanism of embryonic development and to describe and stage the key developmental events. A great deal of work has been done on the staging of embryonic development in decapods of the Crustacea, as shown in Table 2. Although the species are different, there are a lot of similarities in the descriptions of the key events during embryonic development. For example, the staging basis for the cleavage stage, blastocyst stage, gastrulation stage and nauplius stage is almost same, but the difference is that the 7th cleavage of the black tiger prawn and the shrimp Penaeus is an uneven cleavage producing 122 cells, while the 7th cleavage of the mud crab is a surface cleavage producing 128cells. In addition, with the saw-margined blue crab, the stage of the formation of the appendages is subdivided into the 5-pair appendages and the 7-pair appendages, which is likely related to the means of observation.

Monitoring changes in egg coloration stands as the predominant method for assessing the stage of embryonic development within the *S. paramamosain* nursery process. For example, during the cleavage stage, eggs typically exhibit a light orange-yellow hue, while in the later stages, when pigment bands in the compound eyes form, the egg color transitions to brown and then black. A similar trend of color changes was also observed in the study of embryonic development of the orange mud crab (*Scylla olivacea*) (Azra et al., 2015). This method of determining the period of embryonic development just from the egg color is intuitive and does not require any cost. However, it can only give a rough estimate of the period of embryonic development and cannot accurately distinguish the specific stages. The processes occurring at the microscopic level during the embryonic development period seem to be a better explanation of the apparent changes. To that end, this study has systematically demonstrated the embryonic development of *S. pramamosain* through the observations from 1-cell to pre-zoea I periods. When using the light microscope, the emergence of blastopore, formation of attached branches, and compound eye pigment banding could be distinctly observed. In addition, the fluorescence staining method directly enabled observation of the changes in nuclear migration and aggregation without interference from the yolk background color, overcame the blurring of the morphology of the vital organs and appendages in the transparent zone, and provided a good description of cell migration and aggregation during the formation of the blastocyst.

Cleavage refers to the process of high-speed division of the fertilized egg. The result of cleavage is to multiply the number of embryonic cells and prepare the basic conditions for further development and differentiation. Generally, the mode of cleavage of the fertilized egg varies according to species (Chen, 2007). In *S. paramamosain*, the first cleavage was observed to be a complete cleavage, the 2nd to 6th were spiral cleavage, and the 7th to 8th were surface cleavage. In contrast, in the Chinese mitten crab (*Eriocheir sinensis*), the first five cleavages were complete, and it was only from the sixth that surface cleavage began (Du et al., 1992). While in the swimming crab (*Portunus trituberculatus*), surface cleavage occurred from the first cleavage (Xue, 1998). It is worth noting that the *S. paramamosain* embryo split into two unevenly sized cells after the first egg cleavage, which was similar to that observed in the Spotted Shrimp (*Penaeus monodon*), with two unevenly sized cells during the 2-cell stage (Biffis et al., 2009). On the other hand, the difference in size between the two cells was more pronounced for *S. paramamosain*.

The slower division and slightly larger size of the D blastomere than the surrounding crown cells may be well explained by the function of intracellular bodies, enriched with large amounts of RNA, which were thought to play an important role in determining germline fates, causing D blastomere division to be delayed (Pawlak et al., 2010). This delay in cell division may influence the mode of cleavage of the *S. paramamosain* embryo, and the intracellular bodies maybe used as indication of the location of blastoderm emergence to some extent (Biffis et al., 2009). However, whether this indication can be applied in *S. paramamosain* embryonic development needs to be verified in a future study.

The proto-gut of *S. paramamosain* was mainly formed through the invagination of the embryo in the late blastocyst stage, and a transparent zone appeared at one end of the proto-gut, which was consistent with the process of formation of the proto-gut in the swimming crab (*Portunus trituberculatus*) (Xue and Du, 2001) and the Japanese shrimp (*P. japonicus*) (Hudinaga, 1942). In our study, the embryos were found to have cell aggregation in the internal trap area to form the blastopore. Usually, the location of cell aggregation

could generate a transparent zone. This can be explained as due to the rapid depletion of yolk leading to the emergence of a transparent zone (Chen et al., 2021). In other words, the transparent zone was the result of the action of the blastopore in the mud crab embryos.

5 Conclusion

In the current study, the whole embryonic development of *S. paramamosain* has been observed, focusing on the overall color of all the eggs, the morphological changes of individual embryos, and the changes of nuclei migration. The first cleavage of the embryo was an unequal cleavage, and the 2^{nd}-6^{th} cleavages were spiral oogenesis. The larger D cell during the 4-cell period exhibited delayed division relative to the smaller crown cells surrounding it. The 7^{th}-8^{th} cleavages were surface cleavage, and the cleavage furrow was difficult to observe after the sixth oocyte cleavage. In the early gastrulation stage, the embryo concaved inwards to form the blastopore. The cells gathered around the blastopore to further differentiate into different appendage primordia. This work fills a significant gap in our knowledge about the embryonic development of *S. paramamosain* at the nucleus level, and the data obtained will help in the determination of embryo development status and also potentially in the obtaining of high-quality mud crab seedlings.

Data availability statement

The raw data supporting the conclusions of this article will be made available by the authors, without undue reservation.

Ethics statement

The manuscript presents research on animals that do not require ethical approval for their study.

Author contributions

L-KX: Data curation, Methodology, Formal Analysis, Writing – review & editing. K-YM: Data curation, Methodology, Writing – original draft. F-YZ: Formal Analysis, Writing – review & editing. WW: Writing – review & editing, Resources. L-BM: Resources, Writing – review & editing. Z-WJ: Resources, Writing – review & editing. MZ: Writing – review & editing, Software. WC: Software, Writing – review & editing. YF: Software, Writing – review & editing, Funding acquisition. C-YM: Funding acquisition, Writing – review & editing. Z-QL: Data curation, Methodology, Writing – original draft.

Funding

The author(s) declare financial support was received for the research, authorship, and/or publication of this article. This work was funded by the Special Scientific Research Funds for Central Non-profit Institutes, Chinese Academy of Fishery Sciences (2019T07, 2020TD20), China Agriculture Research System (CARS-48), Ningbo Public Welfare Research Project (2023S128), Special Program on Agricultural Aspect of Science and Technology Commission of Ningbo (2019B10010) and the National Infrastructure of Fishery Germplasm Resources.

Conflict of interest

Author ZWJ is employed by Ningbo Yifeng Aquaculture Co. LTD, Ningbo, P.R. China.

The remaining authors declare that the research was conducted in the absence of any commercial or financial relationships that could be construed as a potential conflict of interest.

Publisher's note

Supplementary material

The Supplementary Material for this article can be found online at: https://www.frontiersin.org/articles/10.3389/fmars.2023.1296509/full#supplementary-material

SUPPLEMENTARY FIGURE 1
Changes in female individuals before and after mating, matingless **(A)**, mating **(B)**.

SUPPLEMENTARY FIGURE 2
Overall egg color of ovigerous crabs at the 1-cell stage **(A)**, proto-gut stage **(B)**, nauplii stage **(C)** and pigmentation of the compound eye stage **(D-F)**.

SUPPLEMENTARY FIGURE 3
Morphology of zoea I stage observed under the under light microscopy **(A)** and laser scanning confocal microscope **(B)**.

References

Alwes, F., and Scholtz, G. (2014). The early development of the onychopod cladoceran *Bythotrephes longimanus* (Crustacea, Branchiopoda). *Front. Zool.* 11, 1–23. doi: 10.1186/1742-9994-11-10

Anderson, D. T. (2013). *Embryology and phylogeny in annelids and arthropods: international series of monographs in pure and applied biology zoology*. (Elsevier) 50. doi: 10.2307/2412250

Azra, M. N., Ikhwanuddin, M., Lan, S. S., Abdul, H. N., Siti, N. F., Siti, A. A., et al. (2015). The embryonic development of orange mud crab, *Scylla olivacea* (Herbst 1796) held in the captivity. *Iran. J. Fish. Sci.* 14, 885–895. doi: 10.22092/IJFS.2018.114490

Biffis, C., Alwes, F., and Scholtz, G. (2009). Cleavage and gastrulation of the dendrobranchiate shrimp *Penaeus monodon* (Crustacea, Malacostraca, Decapoda). *Arthropod. Struct. Dev.* 38, 527–540. doi: 10.1016/j.asd.2009.06.003

Bureau of Fisheries and Fishery Management (2023). *China fishery statistical yearbook* (Beijing, China: China Agriculture Press), 22–58.

Chansela, P., Goto-Inoue, N., Zaima, N., Sroyraya, N., Sroyraya, M., Sobhon, P., et al. (2012). Visualization of neuropeptides in paraffin-embedded tissue sections of the central nervous system in the decapod crustacean, *Penaeus monodon*, by imaging mass spectrometry. *Peptides* 34, 10–18. doi: 10.1016/j.peptides.2011.03.021

Chen, J. M. (2007). Foundational studies on the embryonic development of the mud crab, *Scylla serrata* (Forskål). doctoral thesis. (Xiamen, China: Xiamen University).

Chen, S. J., Migaud, H., Shi, C., Song, C. B., Wang, C. L., Ye, Y. F., et al. (2021). Light intensity impacts on growth, molting and oxidative stress of juvenile mud crab *Scylla paramamosain*. *Aquaculture* 545, 737159. doi: 10.1016/j.aquaculture.2021.737159

Du, N. S., Zhao, Y. L., and Lai, W. G. (1992). A study on the embryonic development of the Chinese mitten-handed crab, *Eriocheir sinensis* (Crustacea: Decapoda). *Trans. Chin. Crustacean Soc* 3, 128–135.

Farhadi, A., Huang, Z., Tan, H. Q., Qiu, B. X., Fang, S. B., Ikhwanuddin, M., et al. (2022). Effects of two natural diets on the biochemical compositions of post-mating female mud crab (*Scylla paramamosain*). *Aquacult. Res.* 53, 3504–3515. doi: 10.1111/are.15856

Hertzler, P. L. (2005). Cleavage and gastrulation in the shrimp Penaeus (*Litopenaeus*) *vannamei* (Malacostraca, Decapoda, Dendrobranchiata). *Arthropod. Struct. Dev.* 34, 455–469. doi: 10.1016/j.asd.2005.01.009

Hubble, S. K., and Kirby, R. R. (2007). Transmission electron microscopy of marine crustacean eggs. *Crustaceana* 6, 739–745. doi: 10.1163/156854007781360658

Hudinaga, M. (1942). Reproduction, development and rearing of *Penaeus japonicus* Bate. *Jap. J. Zool.* 10, 305–393. doi: 10.11233/aquaculturesci1953.50.31

Ji, Z. L., Li, R. H., Wang, C. L., Zhang, Z. Y., Zhang, W. J., Mu, C. K., et al. (2022). Effect of long-term low-salinity culture on the survival, growth, and nutrient composition of mud crab *Scylla paramamosain*. *J. Ocean Univ. China* 21, 179–185. doi: 10.1007/s11802-022-4812-x

Liu, Z. M., Wang, G. Z., Li, S. J., and Chen, Z. M. (2018). Mitochondrial respiration rate and enzyme activity of tow population *Scylla paramamosain* during low temperature seasons. *J. Xiamen Univ.* 3, 354–362. doi: 10.6043/j.issn.0438-0479.201710004

Lu, X. P., Ma, L. B., Qiao, Z. G., Zhang, F. Y., and Ma, C. Y. (2009). Population genetic structure of *Scylla paramamosain* from the coast of the Southeastern China based on mtDNA COI sequences. *J. Fish.* 33, 15–23. doi: 10.3321/j.issn:1000-0615.2009.01.003

Luo, J. X., Ren, C., Zhu, T. T., Guo, C., Xie, S. C., Zhang, Y. Y., et al. (2023). High dietary lipid level promotes low salinity adaptation in the marine euryhaline crab (*Scylla paramamosain*). *Anim. Nutr.* 1, 297–307. doi: 10.1016/j.aninu.2022.10.004

Ma, H. Y., Cui, H. Y., Ma, C. Y., and Ma, L. B. (2012). High genetic diversity and low differentiation in mud crab (*Scylla paramamosain*) along the southeastern coast of China revealed by microsatellite markers. *J. Exp. Biol.* 215 (17), 3120–3125. doi: 10.1242/jep.071654

Ma, H. Y., Ma, C. Y., and Ma, L. B. (2011). Population genetic diversity of mud crab (*Scylla paramamosain*) in Hainan Island of China based on mitochondrial DNA. *Biochem. Syst. Ecol.* 39, 434–440. doi: 10.1016/j.bse.2011.06.005

Ma, K. Y., Tian, X. Q., Liu, Z. Q., and Qiu, G. F. (2019). Observations on the embryonic development of the oriental river prawn *Macrobrachium nipponense* (De Haan 1849) (Decapoda: Caridea: Palaemonidae). *J. Crustacean Biol.* 39, 261–266. doi: 10.1093/jcbiol/ruz006

Ma, X. C., and Zhu, F. (2021). The role of myosin-9 in *Scylla paramamosain* against *Vibrio alginolyticus* and white spot syndrome virus infection. *Aquaculture* 531, 735854. doi: 10.1016/j.aquaculture.2020.735854

Mann, R., and Hyne, R. (2008). Embryological development of the Australian amphipod, Melita plumulosa Zeidler 1989 (Amphipoda, Gammaridea, Melitidae). *Crustaceana* 81, 57–66. doi: 10.2307/20107945

Pawlak, J. B., Sellars, M. J., Wood, A., and Hertzler, P. L. (2010). Cleavage and gastrulation in the Kuruma shrimp *Penaeus* (Marsupenaeus) *japonicus* (Bate): a revised cell lineage and identification of a presumptive germ cell marker. *Dev. Growth Differ.* 52, 677–692. doi: 10.1111/j.1440-169X.2010.01205.x

Takano, M., Barinova, A., Sugaya, T., Obata, Y., Watanabe, T., Ikeda, M., et al. (2005). Isolation and characterization of microsatellite DNA markers from mangrove crab, *Scylla paramamosain*. *Mol. Ecol. Notes* 5, 794–795. doi: 10.1111/j.1471-8286.2005.01065.x

Wan, H. F., Zhong, J. Y., Zhang, Z. P., Zou, P. F., and Wang, Y. L. (2021). Discovery of the *Dmrt* gene family members based on transcriptome analysis in mud crab *Scylla paramamosain*. *Gene* 784, 145576. doi: 10.1016/j.gene.2021.145576

Wang, C. X., Wang, R. X., Yang, H. P., Wang, Y. L., and Zhang, Z. P. (2021). Gene cloning and transcriptional regulation of the alkaline and acid phosphatase genes in *Scylla paramamosain*. *Gene* 810, 146057. doi: 10.1016/j.gene.2021.146057

Wang, X. X., Jin, M., Cheng, X., Hu, X. Y., Zhao, M. M., Yuan, Y., et al. (2022). Hepatopancreas transcriptomic and lipidomic analyses reveal the molecular responses of mud crab (*Scylla paramamosain*) to dietary ratio of docosahexaenoic acid to eicosapentaenoic acid. *Aquaculture* 551, 737903. doi: 10.1016/j.aquaculture.2022.737903

Wu, X. G., Liu, Z. J., Yao, G. G., Cheng, Y. X., Yang, X. Z., and Wang, C. L. (2009). Relationship between the organogenesis of hepatopancreas and the yolk utilization during embryonic development of swimming crab, *Portunus trituberculatus*. *Zool. Res.* 30, 449–456. doi: 10.1016/j.aquaculture.2020.7359

Xu, M. Z., Zhang, Q., Dong, L. F., Tong, T., Xie, D., and Su, Q. (2020). Effects of different dietary carbohydrate sources on growth performance, body composition and digestive enzyme activities of juvenile green crab *Scylla paramamosain*. *Fish. Sci.* 39, 175–181. doi: 10.16378/j.cnki.1003-1111.2020.02.004

Xue, J. Z. (1998). Studies on the morphology of the first zoea stage of *Portunus trituberculatus* by sem. *Zool. Res.* 19, 410–411.

Xue, J. Z., and Du, N. S. (2001). Studies on the histology of early embryonic development of. *Portunus trituberculatus*. *J. Ecol.* 34, 69–73. doi: 10.3321/j.issn:0254-5853.2001.01.011

Yao, H. Z., Li, X., Chen, Y. H., Liang, G. L., Gao, L., Wang, H., et al. (2021). Metabolic changes in *Scylla paramamosain* during adaptation to an acute decrease in salinity. *Front. Mar. Sci.* 8. doi: 10.3389/fmars.2021.734519

Zhang, Y., Fang, S. B., Lin, F., Li, S. K., Zheng, H. B., Zhang, Y. L., et al. (2021). Identification and characterization of gene SpDMRT99B and its sex-biased expression profile in the mud crab, *Scylla paramamosain*. *J. Ocean Univ. China* 20, 1495–1504. doi: 10.1007/s11802-021-4765-5